Three-dimensional director structures of defects in Grandjean-Cano wedges of cholesteric liquid crystals studied by fluorescence confocal polarizing microscopy

I. I. Smalyukh and O. D. Lavrentovich*
Chemical Physics Interdisciplinary Program and Liquid Crystal Institute, Kent State University, Kent, Ohio 44242
(Received 19 July 2002; published 11 November 2002)

We use a nondestructive technique of fluorescence confocal polarizing microscopy to visualize three-dimensional director patterns of defects in Grandjean-Cano wedges filled with a cholesteric liquid crystal of pitch $p=5$ μm. Strong surface anchoring of the director causes a stable lattice of dislocations in the bulk. Optical slicing in the vertical cross sections of the wedges allows us to establish the detailed structure of dislocations and their kinks. Dislocations of Burgers vector $b=p/2$ are located in the thin part of the sample, very close to the bisector plane. Their cores are split into a pair of $\tau^{-1/2}$ and $\lambda^{+1/2}$ disclinations. Pairs of $\lambda^{-1/2}$ and $\tau^{+1/2}$ disclinations are observed when the $b=p/2$ dislocation forms a kink. The kinks along the $b=p/2$ dislocations change the level of dislocations by $\pm p/4$ and $\pm p/2$; these kinks are confined to the glide plane and are very long, (5–10) p. Above some critical thickness h_c of the wedge sample, the dislocations are of Burgers vector $b=p$. They are often found away from the bisector plane. The core of $b=p$ dislocations is split into a pair of nonsingular $\lambda^{-1/2}$ and $\lambda^{+1/2}$ disclinations. The kinks along the $b=p$ dislocation are of a typical size p and form cusps in the direction perpendicular to the glide plane. At the cusp, $\lambda^{-1/2}$ and $\lambda^{+1/2}$ disclinations interchange ends. Other defect structures inlude ''Lehmann clusters,'' i.e., dislocations of zero Burgers vector formed by two $\lambda^{-1/2}$ and two $\lambda^{+1/2}$ disclinations and dislocations of nonzero Burgers vector with a core split into more than two disclinations. We employ the coarse-grained Lubensky–de Gennes model of the cholesteric phase to describe some of the observed features. We calculate the elastic energy of a dislocation away from the core, estimate the energy of the core split into disclinations of different types, study the effect of finite sample thickness on the dislocations energy, and calculate the Peach-Koehler elastic forces that occur when a dislocation is shifted from its equilibrium position. Balance of the dilation/compression energy in the wedge and the energy of dislocations defines the value of h_c and allows to estimate the core energy of the dislocations. Finally, we consider the Peierls-Nabarro mechanisms hindering glide of dislocations across the cholesteric layers. Because of the split disclination character of the core, glide is difficult as compared to climb, especially for $b=p$ dislocations.

DOI: 10.1103/PhysRevE.66.051703 PACS number(s): 61.30.Jf, 87.64.Tt, 61.72.Ff, 61.30.−v

I. INTRODUCTION

Cholesteric liquid crystals (CLCs) have a twisted ground state with helical configuration of the director **n**, which specifies the average local orientation of molecules. External fields and surface interactions can easily deform the ideal helicoidal configuration. When the spatial scale of distortions is much larger than the cholesteric pitch p (corresponding to the director twist by 2π), elastic properties of CLCs are similar to those of smectic phases with a one-dimensional periodic structure [1,2]. If a CLC is confined within a finite volume, the equilibrium structure is determined by bulk elas-

stained with *anisometric* dye molecules (in this case, BTBP) that follow the director orientation; (b) the excitation light is *polarized*, usually linearly.

The FCPM setup was assembled on the basis of Olympus Fluoview BX-50 reflective-mode confocal microscope, Fig. 2. The excitation beam (488 nm, Ar laser) is focused by an objective into a small ($<1\ \mu m^3$) volume within the CLC slab. The fluorescent light from this volume is detected by a photomultiplier tube in the spectral region 510–550 nm. A pinhole discriminates against the regions above and below the selected volume [32]. The pinhole size D is adjusted according to magnification and numerical aperture (NA) of the objective; $D=100\ \mu m$ for an immersion oil 60× objective with NA=1.4. The polarizer **P** determines polarization of both the excitation beam $\mathbf{P}_e$, and the detected fluorescent light $\mathbf{P}_f$: $\mathbf{P}_f \| \mathbf{P}_e \| \mathbf{P}$. The beam power is small, ≈120 nW, to avoid light-induced reorientation of the dye-doped LC [33].

For BTBP dye, the fluorescence lifetime $\tau_F=(3.7–3.9)$ ns [34] is smaller than the characteristic time of rotational diffusion $\tau_D \sim 10$ ns, and dye orientations during absorption and emission can be assumed to be close to each other [28]. The FCPM signal, resulting from a sequence of absorption and emission, strongly depends on the angle β between the transition dipole (parallel to the local director **n** in our system) and **P**: $I \sim \cos^4\beta$ [27,28], as both absorption and emission follow the dependency $\cos^2\beta$. The strongest FCPM signal corresponds to $\mathbf{n} \| \mathbf{P}$ ($\beta=0.176$d]TJ -0 9t -0 9ti9.9404rlchapgly

in the vertical component n_z of the director are detected; n_x and n_y

lines with a period $2l$. The distance between the last thin and the first thick line is $1.5l$, Fig. 3(b). The corresponding vertical cross sections reveal the basic features of the defects listed below.

(1) The first line separating 0π and 1π Grandjean zones is a twist disclination, Figs. 4(a) and 5(a), typical of a nematic, as the director experiences a slight splay remaining in the $(x\text{-}z)$ plane to the left of the core and twists by π around the z axis in the region to the right of the core.

(2) The thin lines separating Grandjean zones in the thin part of the sample, $h<h_c$, [such as zones 2π and 3π, Fig. 4(b); 13π and 14π, Fig. 4(c)] are all separated by dislocations with the Burgers vector $\mathbf{b}=(0,0,1)p/2$. Their core is split into disclination pairs $\tau^{-1/2}\lambda^{+1/2}$, Fig. 5(b). Another possible splitting, into $\lambda^{-1/2}\tau^{+1/2}$ pairs, is observed in transient structures when the dislocation $b=p/2$ forms a kink, i.e., a step that brings the dislocation to a different z level, see point (1) in the following subsection. Predominance of $\tau^{-1/2}\lambda^{+1/2}$ pairs over $\lambda^{-1/2}\tau^{+1/2}$ pairs has been explained by Kleman [3]: the singular core in $\tau^{+1/2}$ line is less spread and thus costs more energy as compared to $\tau^{-1/2}$ singular core.

(3) The thick lines at $h>h_c$ are dislocations of Burgers vector $\mathbf{b}=b(0,0,1)$; $b=p$, Fig. 4(d), with the core split into a $\lambda^{-1/2}\lambda^{+1/2}$ pair with a continuous $\mathbf{n}$. Their singular counterparts, $\tau^{-1/2}\tau^{+1/2}$ pairs, are never observed, as the singular core would carry an additional elastic energy $\sim K\ln(p/r_c)$, where K is an average Frank constant and $r_c \ll p$ is the core size of the order of few molecular sizes [5].

(4) The critical thickness h_c of the wedge at which the lattice of $b=p/2$ dislocations is replaced with $b=p$ dislocations depends on the wedge dihedral angle α. Experimentally, for the studied range $5\ \text{mrad}<\alpha<20\ \text{mrad}$, $k=\alpha h_c/p\approx 0.08$, Fig. 6, close to the Durand's data $k\approx 0.12$ [20].

B. Metastable structures: Kinks

Below we describe the defect textures that are not part of the equilibrium defect lattice and appear only as metastable features.

(1) *Kinks along $b=p/2$ dislocations*. In the studied wedges with a strong surface anchoring, both thin and thick lines are located in the bulk of the cell and never at the surfaces. Moreover, the $b=p/2$ dislocations accumulate in the bisector plane or not farther than $p/2$ from it. Initial filling of the cell might form $b=p/2$ dislocations in other locations, but they relatively quickly move to the middle plane. The lines do not glide as the whole, but via kinks, Figs. 7 and 8. There are two types of kinks: kinks of height $\pm p/4$, Fig. 7, and kinks of height $\pm p/2$, Fig. 8. The $\pm p/4$ kinks are more frequent; they are involved in the most common scenario of dislocation glide, in which one $\pm p/4$ kink moves along the dislocation line (along the y axis)

$\lambda^{-1/2}\lambda^{+1/2}$ pair. The vertical cross sections 2–4y-z

tilt, $\lambda^{-1/2}\lambda^{+1/2}$ would transform into a singular $\tau^{-1/2}\tau^{+1/2}$ core. At the cusp, the $\lambda^{-1/2}$ disclination entering the kink from one side transforms into a $\lambda^{+1/2}$ disclination leaving the kink on the other side, Fig. 12. The kink at $b=p$ dislocation, therefore, has a complex structure with a cusp and interchange of the $\lambda^{+1/2}$ and $\lambda^{-1/2}$ disclinations; its size is of the order of p along all three coordinate axes, Fig. 12.

(3) *Thick lines with* $b=p/2$. The thinner part of the wedge

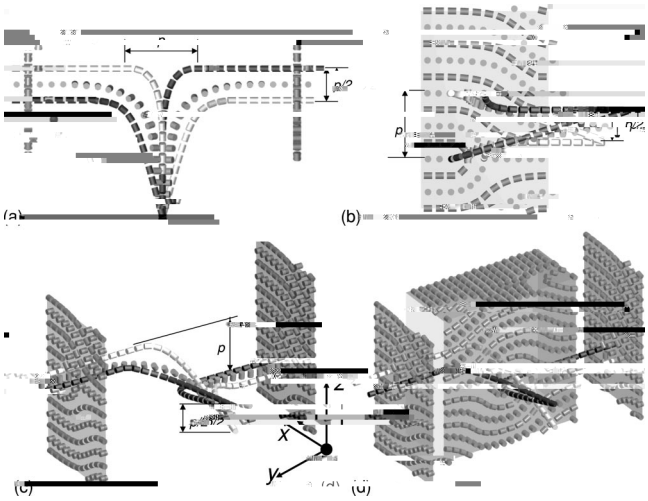

FIG. 12. 3D director field around and at the core of $\lambda^{-1/2}$, $\lambda^{+1/2}$ disclinations in the kink shown in Figs. 9–11, as seen in (a) *x*-*y* projection, (b) *x*-*z* projection, (c), (d) general 3D prospective.

$\lambda^{-1/2}\lambda^{+1/2}$ geometry of the core, similarly to the kink described in point (2).

In mechanical equilibrium, the sum of line tensions of individual dislocations $\mathbf{T}_i$'s at the dislocation node is zero, $\Sigma_i \mathbf{T}_i = 0$, see, e.g., Ref. [6]. The *z* shift is small (a fraction of p) as compared to the radius of curvature of the dislocation, so that the *z* components of $\mathbf{T}_i$'s can be assumed to be much smaller than the *x*,*y* components. In this case, mechanical equilibrium dictates $T_0/T_{p/2} = 2\cos\phi_{p/2}$, $T_0/T_p = 2\cos\phi_p$

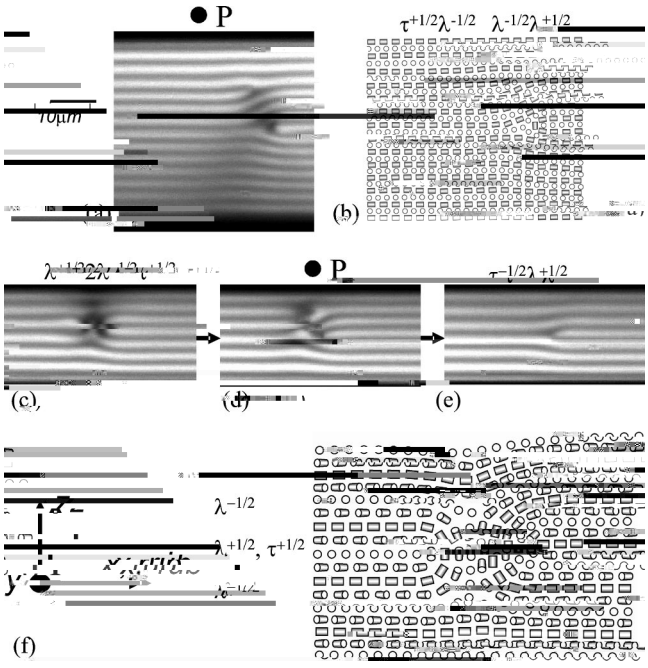

FIG. 13. FCPM vertical cross sections and corresponding director structures of defects with the total Burgers vector $b = p/2$ composed of (a), (b) closely located $\tau^{+1/2}\lambda^{-1/2}$ and $\lambda^{-1/2}\lambda^{+1/2}$ pairs; (c), (d), (e) transformation of the complex core into the $\tau^{-1/2}\lambda^{+1/2}$ pair (e) in the middle of the cell under application of the electric field; (f) shows the director structure in (c).

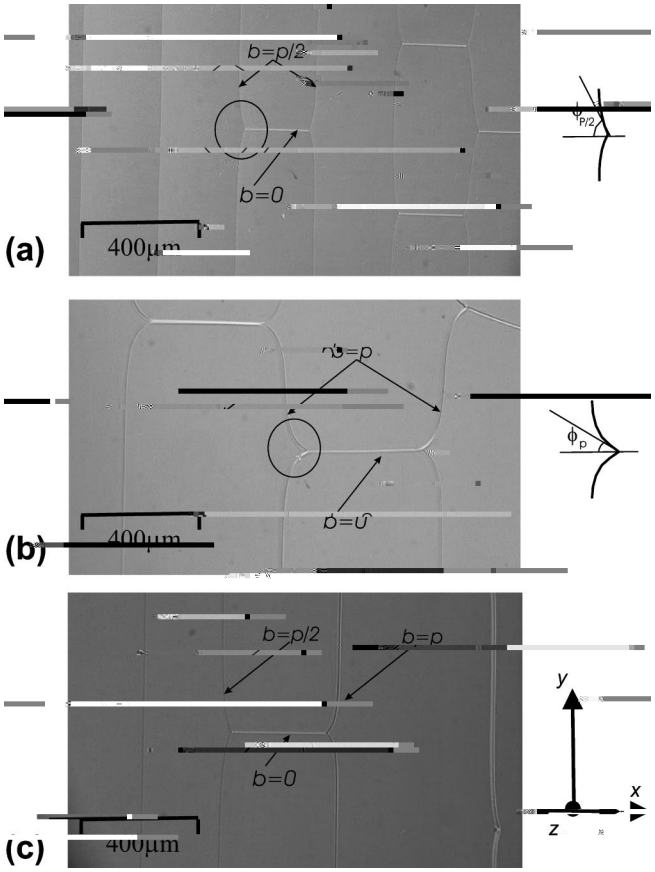

FIG. 14. PM textures of the Grandjean-Cano wedge with defects $b = 0$ connecting (a) $b = p/2$; (b) $b = p$; (c) one $b = p/2$ and one $b = p$ dislocations.

and $T_p/T_{p/2} = \cos\phi_{p/2}/\cos\phi_p$; the angles are defined in Fig. 14. Experimentally, $T_0/T_{p/2} \approx 0.7 \pm 0.2$, $T_0/T_p \approx 1.7 \pm 0.2$, and $T_p/T_{p/2} \approx 0.4 \pm 0.2$. The inequality $T_p < T_{p/2}$ is directly related to the split core structures of the defects, as we shall see in the following section.

IV. ELASTICITY OF DEFECT STRUCTURES

In what follows, we construct an elastic model of defect structures in cholesteric Grandjean-Cano wedge. We treat the CLC as a lamellar mesophase and use the Lubensky-de Gennes coarse-grained theory [1,2], in which the free energy density of layers displacements is of the form

$$f_{nl} = \frac{1}{2}K\left(\frac{\partial^2 u}{\partial x^2}\right)^2 + \frac{1}{2}B\left[\frac{\partial u}{\partial z} - \frac{1}{2}\left(\frac{\partial u}{\partial x}\right)^2\right]^2, \qquad (1)$$

where the compression elastic modulus $B = K_2(2\pi/p)^2$ and the curvature modulus $K = 3K_3/8$ are related to the Frank moduli of twist (K_2) and bend (K_3), respectively. The two constants define an important "penetration" length $\lambda = \sqrt{K/B}$, that equals $(p/2\pi)\sqrt{3K_3/8K_2}$ in the Lubensky–de Gennes model. Experimental values of λ in CLC with p of the order of few microns are indeed close to the theoretical value $\lambda = (p/2\pi)\sqrt{3K_3/8K_2}$ [37]; for our material with $p = 5$ μm, this theoretical value is $\lambda \approx 0.7$ μm. The contribu-

tion $\frac{1}{2}(\partial u/\partial x)^2$ in the compressibility term in Eq. (1) makes the theory nonlinear; in linear approximation,

$$f_l = \frac{1}{2}K\left(\frac{\partial^2 u}{\partial x^2}\right)^2 + \frac{1}{2}B\left(\frac{\partial u}{\partial z}\right)^2 .$$

where $E_{x\text{-}band}$ is the energy of deformations within the infinitely long band $|x| \leq \xi_x$,

$$E_{x\text{-}band} = 2\int_{-\xi_x}^{\xi_x} dx \int_{\xi_z}^{\infty} f_d dz + E_c$$
$$= \frac{Kb^2}{4\pi\xi_x\lambda}\left[-1 + \exp(-2\beta) + \sqrt{\frac{\pi\beta}{2}}\,\mathrm{erf}\sqrt{2\beta}\right] + E_c. \tag{10}$$

Therefore, the far-field energy E_{ff} can be written in two equivalent forms,

$$E_{ff} = \frac{Kb^2}{8\sqrt{2\pi\xi_z}\lambda^{3/2}}\left[\sqrt{\frac{2}{\pi\beta}}\exp(-2\beta) + \mathrm{erf}\ \sqrt{2\beta}\right]$$
$$\equiv \frac{Kb^2}{4\pi\xi_x\lambda}\left[\exp(-2\beta) + \sqrt{\frac{\pi\beta}{2}}\mathrm{erf}\ \sqrt{2\beta}\right]. \tag{11}$$

Note that the relationship between the two forms is that of

torque tending to deviate it from the x-y plane, i.e., to avoid the singular $\tau^{-1/2}\tau^{+1/2}$ core. The same mechanism is responsible for the geometry of kinks along the $b=p$ dislocations, Fig. 12.

As the $\lambda^{-1/2}\lambda^{+1/2}$ dislocations preserve their core structure upon deviations from the y-axis and shift along the z

$$E_B(x_d)=\frac{B}{2}\left[\int_{h_N/\tan\alpha}^{x_d'}dx\int_0^{x\tan\alpha}\left(\frac{\partial u^-}{\partial z}\right)^2dz+\int_{x_d'}^{(h_N+b)/\tan\alpha}dx\int_0^{x\tan\alpha}\left(\frac{\partial u^+}{\partial z}\right)^2dz\right]. \quad (20)$$

Here, $\partial u^-/\partial z = x\tan\alpha/h_N - 1$ and $\partial u^+/\partial z = x\tan\alpha/(h_N+b)-1$. The energy is minimized, $\partial F_B(x_d')/\partial x_d' = 0$, when the dislocation is in the equilibrium position

$$x_{de}'(N)=\frac{2h_N(h_N+b)}{(2h_N+b)\tan\alpha}=\frac{Np(Np+2b)}{2(Np+b)\tan\alpha}. \quad (21)$$

The same result follows from a direct calculation of the Peach-Koehler force, $\mathcal{F}_x^E=-Bb(\partial u^-/\partial z+\partial u^+/\partial z)|_{x_d'}$ that vanishes at $x_d'=x_{de}'$. The distances between two neighboring dislocations at equilibrium are

$$l=\frac{2(N+1)^2p}{(2N+1)(2N+3)\tan\alpha},\quad L=\frac{(N+2)^2p}{(N+1)(N+3)\tan\alpha} \quad (22)$$

for $b=p/2$ and $b=p$ types, respectively; here N refers to the number of cholesteric layers $p/2$ to the left of the dislocation located in the thinner part of the wedge. The separation is a weak function of N; it quickly approaches $b/\tan\alpha$ when $N\to\infty$; even for N as small as 5, the relative difference between $b/\tan\alpha$ and the exact separating distances in Eq. (22) are negligible, less than 2%. In the well-equilibrated samples, dislocations are indeed close to their locations specified by Eq. (21) with separations as in Eq. (22).

A dislocation slightly shifted from its equilibrium position along the x' axis, by $\delta_x = x_d' - x_{de}'$, $|\delta_x| \ll b/2\alpha$, experiences a restoring force $\mathcal{F}_x^E(\delta_x) = -\sigma_{zz}^E b = -\partial E_B(x_{de}'+\delta_x)/\partial\delta_x$ with the direction opposite to the direction of δ_x,

$$\mathcal{F}_x^E(\delta_x)\approx -\frac{Bb\,\delta_x\tan\alpha}{h_N}\,\frac{2h_N+b}{2(h_N+b)}; \quad (23)$$

this force causes dislocation to climbing back to $x'=x_{de}'$. Note here that climb parallel to the layers is easier than glide across the layers, as it preserves the essential geometry of the core and is associated with twist deformations near the core. Because the stresses imposed by the wedge geometry are thickness dependent and small, and because real-time FCPM experiments at this stage are difficult, we leave the discussion of the mobility of dislocations to a future study.

2. Glide

Consider now a case when the dislocation is shifted along the vertical z axis from $z=0$ to some $\delta_z \neq 0$. Here we return to the coordinate system with the x axis along the midplane of the wedge. Because of the boundary conditions $\partial u/\partial x|_{z=\pm h/2}=0$, the dislocation is repelled by the boundary towards the midplane. The corresponding Peach-Koehler force $\mathcal{F}_z^E(z_d)=b\sigma_{zx}^E|_{z=\delta_z}$ can be calculated by placing image dislocations of the same Burgers vector b at both sides of the slab, $z=-mh+(-1)^m\delta_z$ and $z=mh+(-1)^m\delta_z$ [43], where $m=1,2,\ldots,\infty$. The neighboring dislocations to the left and to the right can be neglected, as long as the dihedral angle α and the cell thickness are sufficiently small so that the parabolic regions $x^2 \leqslant 4\lambda|z|$ of layers distortions around neighboring dislocations do not overlap. In the linear approximation, the displacement field u_{zi} caused by the image dislocations is

$$u_{zi}(x,z)=\frac{b}{4}\sum_{m=1}^{\infty}\left[\mathrm{erf}\left(\frac{x}{2\sqrt{\lambda(mh-(-1)^m\delta_z+z)}}\right)-\mathrm{erf}\left(\frac{x}{2\sqrt{\lambda(mh+(-1)^m\delta_z-z)}}\right)\right]. \quad (24)$$

The repelling force $\mathcal{F}_z^E(\delta_z)=-bK(\partial^3 u_{zi}/\partial x^3)|_{z=\delta_z;x=0}$ is then [43]

$$\mathcal{F}_z^E(\delta_z)=\frac{Kb^2}{8\sqrt{\pi}\lambda^{3/2}h^{3/2}}\sum_{m=1.}^{\infty}\left\{\left[m+\frac{\delta_z}{h}[1-(-1)^m]\right]^{-3/2}-\left[m-\frac{\delta_z}{h}[1-(-1)^m]\right]^{-3/2}\right\}. \quad (25)$$

The force vanishes for $\delta_z =$

This experimental feature indicates that the Peierls-Nabarro energy barrier is relatively small as compared to the line tension of the dislocation itself. Imagine a dislocation connecting two points in the bulk of the sample, $A(x_A, z_A)$ and $B(x_B, z_B)$. The smaller the Peierls-Nabarro energy as compared to the line energy of the dislocation, the smaller is ψ: in the limiting case $E_{PN}/E \to 0$, the kink is infinitely long, as the dislocation simply tilts as a whole and preserves the form of a straight line to minimize its length $\sqrt{(x_B - x_A)^2 + (z_B - z_A)^2}$. When the Peierls-Nabarro energy associated with the kink is larger than the line tension, then ψ is large and the kink tends to be short; in the limit $E_{PN}/E \to \infty$, the kink is vertical, of the length $|z_B - z_A|$, it connects two horizontal dislocation segments of total length $|x_B - x_A|$.

For small ψ, one can directly apply the kink model developed for solid crystals [44,45], in which ψ is determined by the (constant) line tension of the edge dislocation $E_{p/2} \approx E_{c,\tau\lambda} \approx (\pi/2) K \ln(p/4r_c)$, Eq. (13), and the Peierls-Nabarro energy $E_{PN}^{p/2} \approx cK$, as $\psi = \sqrt{2E_{PN}^{p/2}/E_{p/2}}$. As $\psi = p/(4w)$ for the $p/4$ kink, one obtains

$$w \approx \frac{p}{4}\sqrt{\frac{E_{p/2}}{2E_{PN}^{p/2}}} \approx \frac{p}{4}\sqrt{\frac{\pi}{4c}\ln\frac{p}{4r_c}}.$$

Using the estimates $p \approx 5$ μm and $r_c \approx 5$ nm, and the experimental result $w \sim (5\text{–}10)p$, one obtains $c \sim (0.3\text{–}1) \times 10^{-2}$. In other words, the core energy variation for the $\tau^{-1/2}\lambda^{+1/2}$ pair along the kink is only a small fraction of the Frank elastic constant K, which is a reasonable conclusion as the $b = p/2$ dislocation can never get rid of the singular core.

In contrast, for a kink along the

(14), depending on the dislocation type. Therefore, the total elastic energies of the two structures are

$$\frac{E_{p/2}}{K} \approx \frac{p^2}{48\lambda^2 \tan\alpha}\left(\frac{1}{N}-\frac{1}{N^2}\right)+\frac{2p}{3\pi\lambda}-\frac{p^{3/2}}{8\sqrt{\pi N}\lambda^{3/2}} + \pi \ln\left(\frac{p}{4r_c}\right)$$

[6] M. Kleman and O. D. Lavrentovich, *Soft Matter Physics: An Introduction* (Springer-Verlag, New York, 2002).
[7] F. Grandjean, C.R. Hebd. Seances Acad. Sci. **172**, 71 (1921).
[8] G. Friedel, Ann. Phys. **18**, 273 (1922).
[9] R. Cano, Bull. Soc. Fr. Mineral. Cristallogr. **90**, 333 (1967).
[10] R. Cano, Bull. Soc. Fr. Mineral. Cristallogr. **91**, 20 (1968).
[11] P. G. de Gennes, C. R. Seances Acad. Sci., Ser. B **266**, 571 (1968).
[12] Orsay Liquid Crystal Group, Phys. Lett. **28A**, 687 (1969).
[13] M. Kleman and J. Friedel, J. Phys. Colloq. **30**, C4-43 (1969).
[14] T. J. Scheffer, Phys. Rev. A **5**, 1327 (1972).
[15] Y. Bouligand, J. Phys. (France) **35**, 959 (1974).
[16] G. Malet and J. C. Martin, J. Phys. **40**, 355 (1979).
[17] S. Masuda, T. Nose, and S. Sato, Liq. Cryst. **20**, 577 (1996).
[18] D. N. Stoenescu, H. T. Nguyen, P. Barois, L. Navailles, M. Nobili, Ph. Martinot-Lagarde, and I. Dozov, Mol. Cryst. Liq. Cryst. **358**, 275 (2001).
[19] R. Holyst and P. Oswald, Int. J. Mod. Phys. B **9**, 1515 (1995).
[20] G. Durand (private communication).
[21] P. Oswald and P. Pieranski, *Les Cristaux Liquides, Tome 1* (Gordon and Breach Science Publishers, Paris, 2000), p. 522.
[22] F. Nalet and J. Prost, Europhys. Lett. , 577 (1974).